

Abstract

Policies to control air quality focus on mitigating emissions of aerosols and their precursors, and other short-lived climate pollutants (SLCPs). On a local scale, these policies will have beneficial impacts on health and crop yields, by reducing particulate matter (PM) and surface ozone concentrations; however, the climate impacts of reducing emissions of SLCPs are less straightforward to predict. In this paper we consider a set of idealised, extreme mitigation strategies, in which the total anthropogenic emissions of individual SLCP emissions species are removed. This provides an upper bound on the potential climate impacts of such air quality strategies.

We focus on evaluating the climate responses to changes in anthropogenic emissions of aerosol precursor species: black carbon (BC), organic carbon (OC) and sulphur dioxide (SO₂). We perform climate integrations with four fully coupled atmosphere-ocean global climate models (AOGCMs), and examine the effects on global and regional climate of removing the total land-based anthropogenic emissions of each of the three aerosol precursor species.

We find that the SO₂ emissions reductions lead to the strongest response, with all three models showing an increase in surface temperature focussed in the northern hemisphere high latitudes, and a corresponding increase in global mean precipitation and run-off. Changes in precipitation and run-off patterns are driven mostly by a northward shift in the ITCZ, consistent with the hemispherically asymmetric warming pattern driven by the emissions changes. The BC and OC emissions reductions give a much weaker forcing signal, and there is some disagreement between models in the sign of the climate responses to these perturbations. These differences between models are due largely to natural variability in sea-ice extent, circulation patterns and cloud changes. This large natural variability component to the signal when the ocean circulation and sea-ice are free-running means that the BC and OC mitigation measures do not necessarily lead to a discernible climate response.

Climate responses to anthropogenic emissions

L. H. Baker et al.

Title Page

Abstract

Introduction

Conclusions

References

Tables

Figures



Back

Close

Full Screen / Esc

Printer-friendly Version

Interactive Discussion



1 Introduction

Anthropogenic emissions of short-lived climate pollutants (SLCPs), such as aerosols and tropospheric ozone precursors, contribute to poor air quality by increasing particulate matter (PM) and surface ozone concentrations. These are damaging to both human health and agriculture (HTAP, 2010). Air quality policies therefore aim to reduce emissions of SLCPs. While these policies will have a beneficial impact on air quality, the climate impacts of reducing emissions of SCLPs are less clear.

SLCPs have relatively short atmospheric lifetimes compared with well-mixed greenhouse gases (WMGHGs) such as CO₂, remaining in the atmosphere for only days to months. The impacts of SLCP emissions on climate therefore occur on relatively short timescales of less than 30 yr (Collins et al., 2013). The short atmospheric lifetime of SLCPs means that their distribution is not homogeneous as in the case of WMGHGs, and concentrations tend to be highest nearer to source regions. Therefore the resulting forcing patterns are also inhomogeneous, and diagnosing the regional and global climate impacts is much more complex than for WMGHGs (Shindell et al., 2009; Shindell and Faluvegi, 2009). In particular the majority of anthropogenic emissions of SLCPs are in the northern hemisphere, so the forcing is much stronger in the northern hemisphere than the southern hemisphere (Shindell, 2014). The direct effects and the indirect and semi-direct effects of aerosols on clouds bring further inhomogeneities, so the resulting impacts of SLCPs on regional and global climate are quite different to those for the WMGHGs.

In this paper we focus on aerosol and aerosol precursor emissions, namely black carbon (BC), organic carbon (OC) and sulphur dioxide (SO₂), which is a precursor to sulphate (SO₄) aerosol formation.

The effects of anthropogenic aerosols on climate are complex. Scattering aerosols (such as SO₄ and OC) reflect downwelling solar radiation back out of the atmosphere, resulting in a negative top-of-atmosphere (TOA) short-wave (SW) forcing. This reduction in the solar radiation absorbed by the atmosphere results in a decrease in global

Climate responses to anthropogenic emissions

L. H. Baker et al.

Title Page

Abstract

Introduction

Conclusions

References

Tables

Figures



Back

Close

Full Screen / Esc

Printer-friendly Version

Interactive Discussion



mean surface temperature. Hydrophilic aerosols also provide cloud condensation nuclei (CCN), which increases cloud albedo and alters other properties including cloud amount, and further contributes to the negative forcing (Boucher et al., 2013). In contrast, BC aerosol absorbs incoming solar radiation, which means it has a net warming effect on the atmosphere and gives a positive TOA SW forcing. The local impact of BC on the surface temperature is dependent on the altitude of the BC: low-level BC can warm the surface, whereas higher-level BC can reduce the surface temperature by absorbing part of the downwelling solar radiation before it reaches the surface (Ramanathan and Carmichael, 2008). Even in cases where the surface is cooled locally, the additional solar radiation absorbed by the BC results in a warming effect on the higher atmosphere. BC located near to clouds can cause evaporation of clouds, known as the semi-direct effects (Koch and Del Genio, 2010). However, depending on the exact location of the BC and type of cloud, BC can either increase or decrease cloud cover via various different mechanisms (Ban-Weiss et al., 2012), so the net impact on clouds of a given atmospheric distribution of BC is highly complex. BC aloft causes stabilisation of the atmosphere, which can lead to increased stratocumulous clouds (Koch and Del Genio, 2010). BC also has important impacts at high latitudes when it is deposited on snow, as it decreases the albedo of the snow surface (Ramanathan and Carmichael, 2008), and can enhance snow melt by absorbing solar radiation after it is deposited (Flanner et al., 2007). However, the impacts of BC forcing in the Arctic on surface temperature are complex, as the result is highly dependent on the altitude and location of the forcing (Sand et al., 2013a, b; Flanner, 2013).

Aerosols also affect precipitation (e.g. Kristjánsson et al., 2005; Ming et al., 2010). On a global scale, we might expect the precipitation to change in proportion to a given temperature change driven by aerosol forcing, due to the increased amount of water vapour that the atmosphere can hold (Lambert and Webb, 2008). However, since the direct, semi-direct and indirect effects of aerosols will change precipitation patterns, this does not necessarily hold locally. Hydrophilic aerosol species can reduce precipitation locally, by enhancing cloud droplet nucleation, which allows more smaller cloud

Climate responses to anthropogenic emissions

L. H. Baker et al.

[Title Page](#)[Abstract](#)[Introduction](#)[Conclusions](#)[References](#)[Tables](#)[Figures](#)[Back](#)[Close](#)[Full Screen / Esc](#)[Printer-friendly Version](#)[Interactive Discussion](#)

droplets to form but inhibits the amount of droplets that become large enough to form precipitation. Other effects such as convective invigoration that might also affect precipitation (Rosenfeld et al., 2008) are not parameterised in the models assessed here. BC has more complex effects on precipitation patterns since it warms the atmosphere (Andrews et al., 2010) but can either warm or cool the surface, which will increase or reduce the amount of surface evaporation and resulting precipitation (Ming et al., 2010). The net effect on precipitation is therefore dependent on the region and vertical profile of the BC aerosol (Andrews et al., 2010; Ban-Weiss et al., 2012; Kvalevåg et al., 2013). Furthermore the hemispherically asymmetric forcing from anthropogenic aerosol emissions impacts the temperature in the northern hemisphere more than in the southern hemisphere, leading to a meridional shift in the Intertropical Convergence Zone (ITCZ) towards the warmer hemisphere (e.g. Kang et al., 2008; Ceppi et al., 2013), which will impact local precipitation in the tropics and the monsoon regions (Ming and Ramaswamy, 2009). Several studies have shown that anthropogenic aerosol emissions in recent decades have contributed to the weakening of the northern hemisphere monsoon (e.g. Bollasina et al., 2011; Polson et al., 2014). Aerosols also impact the hydrological cycle by reducing the amount of solar radiation reaching the surface, a process known as solar dimming (Gedney et al., 2014). Solar dimming acts to reduce evaporation, and results in increased run-off and suppressed evapotranspiration.

Policies to reduce anthropogenic aerosol emissions are generally designed to have positive impacts on air quality by reducing PM concentrations; however they can have mixed effects on climate. Reducing SO₂ and OC emissions is expected to have a detrimental effect on climate in the sense that such measures would be contributing to an increase in global temperature; however the impacts on precipitation patterns could be beneficial, for example by preventing further reduction in monsoon precipitation. In contrast, mitigating BC emissions is expected to reduce global temperature, while the resulting impacts on precipitation are less clear. It is therefore important to evaluate the climate impacts of individual aerosol species in order to evaluate these effects.

Climate responses to anthropogenic emissions

L. H. Baker et al.

[Title Page](#)[Abstract](#)[Introduction](#)[Conclusions](#)[References](#)[Tables](#)[Figures](#)[Back](#)[Close](#)[Full Screen / Esc](#)[Printer-friendly Version](#)[Interactive Discussion](#)

Climate responses to anthropogenic emissions

L. H. Baker et al.

Title Page

Abstract

Introduction

Conclusions

References

Tables

Figures



Back

Close

Full Screen / Esc

Printer-friendly Version

Interactive Discussion



Here we assess the climate impacts of removing the total land-based anthropogenic emissions of each of SO₂, OC and BC in three coupled climate models with interactive chemistry and aerosols. The multi-model nature of this work gives greater confidence in the results since we are not drawing conclusions based on results from just one model. The 100% perturbations were used in order to achieve a strong enough forcing signal. Results from atmosphere-only simulations (e.g. Bellouin et al., 2015) suggest that the removal of anthropogenic SO₂ and OC emissions will lead to a positive forcing and a global temperature increase, while removing anthropogenic BC emissions will lead to a negative forcing and a global temperature decrease. Using coupled models allows the ocean circulation and heat uptake, and sea-ice extent, to respond to the atmospheric changes from the emissions perturbations. We assess the resulting changes in temperature, circulation patterns, precipitation and run-off both globally and regionally.

In Sect. 2, the climate models, experimental setup and emissions datasets are described. In Sect. 3 the climate impacts of removing the emissions of individual anthropogenic aerosol species are presented. These results are discussed further in Sect. 4, and conclusions are given in Sect. 5.

2 Methodology

2.1 Description of models

The three main models used are HadGEM3, ECHAM6-HAM2 and NorESM1-M. HadGEM3 and NorESM1-M have interactive aerosols and chemistry; ECHAM6-HAM2 has interactive aerosols but does not include interactive chemistry. Therefore in HadGEM3 and NorESM1-M, changes in the aerosols can affect the chemistry via changes in oxidation of SO₂ and changing the available surface for heterogeneous chemistry; these processes will directly and indirectly affect O₃ and OH. The fact that ECHAM6-HAM2 does not include interactive chemistry is expected to lead to only mi-

nor differences from the other two models with interactive chemistry with regard to the radiative and climate effects of aerosol and aerosol precursor emissions. For the BC perturbation experiments some additional simulations were performed: one extra ensemble member was run by NorESM1-M, and two ensemble members were run by
5 NCAR CESM 1.0.4/CAM4.

HadGEM3 is the Hadley Centre Global Environment Model version 3 (Hewitt et al., 2011). The atmosphere component has a horizontal resolution of $1.875^\circ \times 1.25^\circ$ and 85 vertical levels extending to 85 km in height (of which 50 are below 18 km). The atmosphere is coupled to the NEMO ocean modelling framework with a horizontal
10 resolution of 1.0° and 75 vertical levels, and to the CICE sea-ice model (Hunke and Lipscomb, 2008). The UKCA TropIsop scheme is used to model gas-phase chemistry. This treats 55 chemical species (37 of which are transported) including hydrocarbons up to propane, and isoprene and its degradation products (O'Connor et al., 2014). Atmospheric gas and aerosol tracers are advected using the same semi-Lagrangian
15 advection scheme as used for the physical climate variables. Parameterized transport such as boundary layer mixing and convection is also as used for the physical climate variables. Aerosols are modelled by the UKCA-Mode aerosol scheme (Mann et al., 2010; Abdul-Razzak and Ghan, 2000). This models the internal mixing of SO_4 , OC, BC, dust and sea-salt using a two-moment modal approach and dynamically evolving particle
20 size distributions. There are seven modes: four soluble (nucleation to coarse) and three insoluble (Aitken to coarse). Aerosol processes are simulated in a size-resolved manner, including primary emissions, secondary particle formation by binary homogeneous nucleation of sulphuric acid and water, particle growth by coagulation, condensation, and cloud-processing, and removal by dry deposition, in-cloud and below-cloud scavenging. The radiative impact from aerosols is calculated using the Edwards-Slingo
25 radiation scheme (Edwards and Slingo, 1996).

ECHAM6-HAM2 is the European Centre for Medium-Range Weather Forecasts Hamburg model version 6 (Stevens et al., 2013). The atmospheric simulations were made using the ECHAM6 GCM with a horizontal resolution of T63 (about $1.8^\circ \times 1.8^\circ$)

Climate responses to anthropogenic emissions

L. H. Baker et al.

Title Page

Abstract

Introduction

Conclusions

References

Tables

Figures



Back

Close

Full Screen / Esc

Printer-friendly Version

Interactive Discussion



Climate responses to anthropogenic emissions

L. H. Baker et al.

Title Page

Abstract

Introduction

Conclusions

References

Tables

Figures



Back

Close

Full Screen / Esc

Printer-friendly Version

Interactive Discussion



ospheric gas-phase chemistry from MOZART (Emmons et al., 2010), which treats around 80 gaseous species. This coupling allows for a more explicit description of the formation of secondary aerosol (SO_4 and secondary OM). The radiative forcing from aerosols is calculated using the Collins (2001) radiation scheme. In the fully coupled NorESM1-M, albedo-effects of BC and mineral dust aerosols deposited on snow and sea-ice are also taken into account.

NCAR CESM 1.0.4/CAM4 is the National Center for Atmospheric Research Community Earth System Model (Gent et al., 2011) run with the Community Atmosphere Model version 4 (Neale et al., 2011). The atmospheric component is set up here with a horizontal resolution of $1.9^\circ \times 2.5^\circ$, and 26 vertical layers (extending from the surface to 2.19 hPa). CAM4 is coupled to a full ocean model (Danabasoglu et al., 2012), which is based on the Parallel Ocean Program version 2 (Smith et al., 2010), to the CICE4 sea ice model (Hunke and Lipscomb, 2008), and the CLM4 land model (Lawrence et al., 2011). Here, the model has been run without interactive chemistry and aerosols, and instead used prescribed 3-D monthly mean concentrations of ozone and aerosols from the Oslo Chemistry-Transport model version 2 (OsloCTM2) (Søvde et al., 2008; Myhre et al., 2009). OsloCTM2 is driven by meteorological data from the ECMWF-IFS model, and has been run with T42 (approximately $2.8^\circ \times 2.8^\circ$) horizontal resolution and 60 vertical layers (extending from the surface to 0.1 hPa). In CAM4, the direct and semi-direct aerosol effects of BC are included, while indirect aerosol effects and the effect of BC deposited on snow and ice are not included.

Hereafter we refer to the four models discussed above as HadGEM, ECHAM-HAM, NorESM and CESM-CAM4, respectively.

2.2 Experimental setup and emissions

Each of the three main models (HadGEM, ECHAM-HAM and NorESM) ran a control simulation and a set of three perturbation experiments in which the land-based anthropogenic component of a single aerosol emission species was removed. In addition, NorESM ran a second control and perturbed BC experiment, and CESM-CAM4 ran

Climate responses to anthropogenic emissions

L. H. Baker et al.

Title Page

Abstract

Introduction

Conclusions

References

Tables

Figures



Back

Close

Full Screen / Esc

Printer-friendly Version

Interactive Discussion



two control and two perturbed BC experiments. The control and perturbed simulations were run for 50 yr (after an initial spin-up period of several decades), in order to separate a robust signal from the interannual variability. The 50-year integration length was deemed sufficient based on previous studies, e.g. Kristjánsson et al. (2005) performed integrations of length 40 yr after 10 yr of spin-up, and Pausata et al. (2014) performed integrations of length 30 yr after 30 yr of spin-up. Furthermore, Olivié et al. (2012) showed that most of the temperature response to a step CO₂ perturbation in AOGCMs is achieved within around the first 10 yr or so (the Cx2 case in their Fig. 1), after which the temperature remains relatively constant, with only a very gradual continued increase towards the equilibrium response temperature.

We focus on global mean and zonal mean values of the following climate variables: surface temperature, precipitation, and run-off. We also examine the top-of-atmosphere (TOA) short-wave (SW) fluxes to aid understanding of these results. This is not the same as the TOA SW forcing in prescribed-SST simulations since in the coupled simulations it includes the fast and slow cloud and sea-ice responses and feedbacks. It is useful in understanding the causes of changes in climate variables, particularly on regional scales.

The control simulations have present-day anthropogenic emissions of SLCP species from the ECLIPSE emission dataset V4.0a (Klimont et al., 2013, 2015) (for the year 2008 for all models except CESM-CAM4 which used 2000). Biomass burning emissions are from the GFED3 emissions dataset (<http://www.globalfiredata.org>) for the year 2005 (in ECHAM-HAM and NorESM) and 2008 (in HadGEM and CESM-CAM4), and are not perturbed. Sea-salt and dust aerosol emissions are interactive in HadGEM and ECHAM-HAM; in NorESM, dust emissions are prescribed from a climatology but sea-salt emissions are interactive; and in CESM-CAM4 both dust and sea-salt emissions are prescribed from a climatology. Other natural emissions are included, and are not perturbed. The concentrations of WMGHGs are also kept fixed at present-day levels in HadGEM, NorESM and CESM-CAM4, and in ECHAM-HAM are fixed at pre-industrial (1850) levels. The surface methane concentration is also prescribed at

present-day levels in HadGEM and NorESM and at pre-industrial levels in ECHAM-HAM. For ECHAM-HAM, the pre-industrial greenhouse gas concentrations were chosen since the model was spun up to equilibrium for this case, and a new spin-up for increased levels of greenhouse gas concentrations would have been computationally too costly. Since only differences between experiments and control simulations are considered here, no large effect caused by the differences in greenhouse gas concentrations is expected.

Figure 1 shows the emissions of BC, OC and SO₂, divided into the anthropogenic emissions that are perturbed in the experiments (left column) and other emissions that are input to the model (natural, biomass burning and shipping; right column). The strongest anthropogenic emissions of all three species are mostly concentrated over China, India, Europe, the eastern US and parts of Africa and South America.

Despite all the models having the same emissions input, there is a large discrepancy between models in the vertical distribution of aerosols in the atmosphere, and in the total aerosol burden, which is typical for current global aerosol models (Textor et al., 2007). HadGEM and ECHAM-HAM have relatively low total burdens of BC compared with NorESM and CESM-CAM4 (Table 1). In contrast, NorESM and CESM-CAM4 have relatively low burdens of SO₄ compared with HadGEM and ECHAM-HAM. The OC burden in NorESM is considerably higher than in the other three models. Figure 2 shows vertical sections of the annual average, zonal mean BC mass mixing ratio in the control simulation for each of the models considered. HadGEM and ECHAM-HAM (Fig. 2a and b) have low concentrations of BC at high altitude, which means there is less BC above clouds. In contrast, NorESM and CESM-CAM4 show high BC concentrations extending to above 200 hPa throughout most of the northern hemisphere and southern hemisphere tropics (Fig. 2c and d). This has implications for the impact that removing anthropogenic BC emissions may have. BC at high altitude can have very strong direct effects if it is located above high-albedo cloud surfaces. In the models with higher concentrations of BC at high levels in the control simulations, more of this high-level BC can be removed in the BC perturbation experiment, leading to a larger change

Climate responses to anthropogenic emissions

L. H. Baker et al.

[Title Page](#)[Abstract](#)[Introduction](#)[Conclusions](#)[References](#)[Tables](#)[Figures](#)[Back](#)[Close](#)[Full Screen / Esc](#)[Printer-friendly Version](#)[Interactive Discussion](#)

in BC direct forcing. There are also differences in the vertical distribution of OC and SO₄ between models (not shown) but as these are scattering, rather than absorbing, aerosols the impact of the vertical distribution of the aerosol will have less of an impact on the results.

Figure 3 shows the annual average global mean surface temperature in the control simulations for each of the models. ECHAM-HAM has a lower mean temperature than the other models due to its pre-industrial WMOGHG and methane concentrations. CESM-CAM4 has a higher mean temperature than the others. ECHAM-HAM has a slight negative drift in surface temperature over the integration period, while both NorESM ensemble members have a slight positive drift; the other two models remain relatively stable.

3 Results

In this section we examine the climate responses to perturbing each of the emissions species. The results shown are annual means averaged over the 50-year integration period for each model. Note that since we are interested the impacts that removing anthropogenic emissions would have, the plots show the perturbation run (i.e. the run with emissions removed) minus the control run. This is different from most other studies, which in general tend to show, e.g. the forcing of the present-day aerosol compared with a pre-industrial background state.

3.1 Response to perturbing SO₂ emissions

All three models show an increase in global mean surface temperature as a result of removing anthropogenic SO₂ emissions: HadGEM and ECHAM-HAM show almost equal temperature increases while NorESM warms by approximately half this value (Fig. 4a). The multi-model mean global mean surface temperature increases by 0.69 K. The zonal mean temperature change is positive at all latitudes, and increases with in-

Climate responses to anthropogenic emissions

L. H. Baker et al.

Title Page

Abstract

Introduction

Conclusions

References

Tables

Figures



Back

Close

Full Screen / Esc

Printer-friendly Version

Interactive Discussion



creasing latitude, with a multi-model mean, zonal mean temperature increase of around 2.5 K at the North Pole (Fig. 5b). Figure 5a shows warming over almost all areas of the globe, including all land areas. The three models are in agreement on the sign of this temperature response throughout almost all the Northern Hemisphere, and much of the Southern Hemisphere. Most of the Northern Hemisphere land shows warming of at least 1 K, with some northern regions exceeding 2 K.

These temperature responses can be understood further by comparison with the TOA SW flux changes. The global mean TOA SW flux change is positive for all three model simulations (Fig. 4b). HadGEM, which has the strongest temperature response, also has the largest change in TOA SW flux, while NorESM, which has the weakest temperature response, has the smallest change in TOA SW flux. The strongest increase in TOA SW flux change occurs in the Northern Hemisphere mid-latitudes, where the anthropogenic emissions are largest (Fig. 6b). There is good agreement between the three models in the zonal distribution of TOA SW flux change, although NorESM shows smaller values in the Northern Hemisphere, which may explain the weaker temperature increase in this model compared to the others. There is agreement between the three models in the positive sign of the TOA SW flux change throughout most of the Northern Hemisphere (Fig. 6a). There are regions of strong TOA SW flux change over Europe, the eastern USA and China, which correspond to locations with the largest anthropogenic emissions. Over Europe and the eastern USA, this explains the relatively strong warming in these regions (Fig. 5a). The positive TOA SW flux change over China also extends in a band over the North Pacific. This is likely to be caused by changes in cloud cover due to the reduction in aerosol emissions in China, in agreement with the results of Wang et al. (2014) which showed that Chinese aerosols increased cloud cover over the North Pacific. A similar region of positive TOA SW flux change also occurs over the North Atlantic, which could similarly be due to aerosol-induced cloud changes over this region resulting from the aerosol emissions reductions over the eastern USA. The regions of negative TOA SW flux change in the Pacific and Atlantic just north of the equator relate to a northward shift in the ITCZ, which increases the cloud

Climate responses to anthropogenic emissions

L. H. Baker et al.

[Title Page](#)[Abstract](#)[Introduction](#)[Conclusions](#)[References](#)[Tables](#)[Figures](#)[Back](#)[Close](#)[Full Screen / Esc](#)[Printer-friendly Version](#)[Interactive Discussion](#)

cover north of the equator. This northward ITCZ shift is expected due to the hemispherically asymmetric warming.

At high northern hemisphere latitudes there are regions of enhanced warming and corresponding increased TOA SW flux (Figs. 5a and 6a), the most pronounced being over the ocean north of Europe. These correspond to regions with large reductions in sea-ice (not shown). All three models agree on a large loss of Arctic sea-ice, due to the strong northern hemisphere warming. In the southern hemisphere, all three models actually show a region of increased sea-ice east of the Antarctic Peninsula, which explains the reduced temperatures and decreased TOA SW flux there.

The removal of anthropogenic SO_2 emissions results in an increase in global mean precipitation (Fig. 4c). This increase is expected due to the increased surface temperature. The multi-model mean percentage precipitation change per unit warming can be calculated from Table 2 as $2.50\% \text{K}^{-1}$, which is consistent with the value for SO_4 found by Andrews et al. (2010) ($2.46 \pm 0.11\% \text{K}^{-1}$). While there is a global increase in precipitation, the southern hemisphere actually shows an overall decrease in precipitation (Fig. 7b). This is mostly due to the northward shift in the ITCZ (discussed above), which can be seen as a clear dipole in precipitation change about the equator. All three models agree on the northward shift in tropical precipitation over the ITCZ regions (Fig. 7a). There is a relatively strong increase in precipitation over India and China, collocated with regions of high anthropogenic emissions of SO_2 . There is a clear increase in precipitation in the Indian monsoon region, which is consistent with the findings that anthropogenic aerosol has caused a weakening of the summer monsoon (Bollasina et al., 2011; Polson et al., 2014). There are broad regions over Russia and northern America with increased precipitation corresponding to increased surface temperature (and therefore more available moisture through evaporation).

There is an increase in global run-off, which is consistent with the increased global mean surface temperature and precipitation (Fig. 4d). Spatially these changes are strongly linked to the changes in precipitation patterns (Fig. 8a compared with Fig. 7a). The most coherent changes in run-off occur in the tropics, due to the shift in the ITCZ,

Climate responses to anthropogenic emissions

L. H. Baker et al.

Title Page

Abstract

Introduction

Conclusions

References

Tables

Figures



Back

Close

Full Screen / Esc

Printer-friendly Version

Interactive Discussion



Climate responses to anthropogenic emissions

L. H. Baker et al.

Title Page

Abstract

Introduction

Conclusions

References

Tables

Figures



Back

Close

Full Screen / Esc

Printer-friendly Version

Interactive Discussion



notably an increase in run-off over India and a band of increased run-off over the Sahel, both of which are due to collocated increases in precipitation. Over Europe and much of North America there is a decrease in run-off, which is a result of increased surface temperature, increased solar radiation reaching the surface, but decreased precipitation in these regions, which will increase evaporation but reduce available moisture reaching the surface. This is consistent with the work of Gedney et al. (2014), who attributed increased run-off in heavily polluted parts of Europe to high aerosol concentrations. It is interesting to note that ECHAM-HAM has a much smaller global change in run-off than the other two models, despite having the largest increases in precipitation and temperature (Fig. 4a, c and d). Inspection of spatial maps of run-off for ECHAM-HAM (not shown) shows that this is due to a relatively large decrease in run-off over South America compared with the other models, but fairly similar changes elsewhere.

Overall the models agree on the climate response to removing anthropogenic SO₂ emissions, showing northern hemisphere warming and a northward shift in the ITCZ.

3.2 Response to perturbing black carbon emissions

For the BC perturbation experiments, we consider, in addition to the original simulations from HadGEM, ECHAM-HAM and NorESM, one extra ensemble member from NorESM, and two ensemble members from CESM-CAM4. For the calculations of multi-model means, each of these additional members is weighted equally with the other model simulations.

The response to removing anthropogenic BC emissions is much smaller overall than the response to perturbing SO₂ emissions (Fig. 4). All the models except HadGEM show a net decrease in global mean surface temperature, although CESM-CAM4 member 2 shows only a very small decrease (Fig. 4a). This results in a small negative multi-model mean value for the global surface temperature response. A similar pattern is seen for the change in TOA SW flux (Fig. 4b), although it is interesting to note that CESM-CAM4 member 2 has a relatively strong negative TOA SW flux change compared to its very small temperature response.

Climate responses to anthropogenic emissions

L. H. Baker et al.

Title Page

Abstract

Introduction

Conclusions

References

Tables

Figures



Back

Close

Full Screen / Esc

Printer-friendly Version

Interactive Discussion



The multi-model mean temperature response is within ± 0.5 K everywhere (Fig. 5c). There are stippled regions (where at least five of the six ensemble members agree on the sign) in large parts of the southern hemisphere ocean and the tropical Pacific, but much less stippling in the northern hemisphere. The TOA SW flux change is also relatively small everywhere (Fig. 6c). There are stippled regions over areas with high anthropogenic BC emissions, with the strongest TOA SW flux decrease over northern India.

The small multi-model mean temperature and TOA SW flux responses are the result of conflicting regional responses in the different models, rather than weak responses in each model. This can be seen in Fig. 5d, which shows the range of zonal mean temperature responses between models. Both NorESM members show relatively strong cooling, which is stronger towards high latitudes, reaching around -0.4 K at the north pole. In contrast, HadGEM shows warming of a similar magnitude, again increasing towards high latitudes and reaching 0.4 K at the north pole. ECHAM-HAM shows a weak response in general but a small increase towards the north pole. The two CESM-CAM4 members show different behaviour: member 1 shows cooling at most latitudes, peaking at around 60°N and 70°S ; member 2 shows warming increasing throughout the northern hemisphere mid- to high-altitudes and reaching 0.6 K at the north pole.

The spatial responses in each of the model simulations can be seen in Figs. S1–S3 in the Supplement. HadGEM shows warming in the Arctic and over most of the northern hemisphere mid-latitudes, including Europe, which is unexpected since anthropogenic BC emissions are relatively large there (Fig. S1a). CESM-CAM4 member 2 (Fig. S3b) also shows warming over the Arctic, but not over the rest of the northern hemisphere. In contrast, both NorESM members (Fig. S2a and b) show robust cooling over these regions, while ECHAM-HAM (Fig. S1a) shows cooling over some areas of the mid-latitudes but warming over much of the Arctic. CESM-CAM4 member 1 shows weak cooling over some mid- and high-latitude regions (Fig. S3a).

The zonal mean TOA SW flux change also shows large differences between models (Fig. 6d), which helps to explain the range of temperature responses in each model

in the northern hemisphere. The three simulations that show warming in the northern hemisphere high-latitudes (HadGEM, ECHAM-HAM and CESM-CAM4 member 2) all show positive TOA SW flux changes in the northern hemisphere, peaking between around 60 and 70°N (Fig. 6d). These high-latitude regions of increased TOA SW flux can be seen in Figs. S1c and d, and S3d. Comparison with the respective sea-ice changes (Figs. S1e and f, and S3f) shows a strong correlation between increased TOA SW flux and decreased sea-ice. In contrast, for both the NorESM members, which show cooling in the northern hemisphere, there is a clear decrease in TOA SW flux over most of the northern hemisphere high-latitudes (Figs. S2c and d), and collocated increases in sea-ice (Figs. S2e and f). CESM-CAM4 member 1 shows only relatively small changes in TOA SW fluxes (Fig. S3c), and smaller changes in Arctic sea-ice (Fig. S3e). All the models show decreased TOA SW flux over India and China, consistent with the location of the strongest BC emissions reductions (middle panels of Figs. S1–S3). All models except HadGEM also show a decrease in TOA SW flux over Europe, which is expected since the anthropogenic emissions of BC are relatively strong here. The region of positive TOA SW flux change over Europe in HadGEM is in fact a result of a combination of reduced cloud cover and reduced snow cover over Northern Europe (not shown); these changes are likely due to circulation changes, and their combined effect is enough to more than balance the negative forcing from local removal of BC.

The global mean precipitation response to removing anthropogenic BC emissions is relatively small (Fig. 4c). Despite the different signs of temperature response, the global precipitation increases in all the models. This is not surprising since the removal of BC from the atmosphere will lead to a negative atmospheric forcing, which in turn is expected to lead to increased precipitation (Andrews et al., 2010). Both NorESM members show a pronounced southward shift in the position of the ITCZ, which is consistent with the cooling in the northern hemisphere in these simulations (Fig. 7d). HadGEM shows a weak northward shift in the ITCZ, while the other models do not show a coherent shift in its position. The opposing direction of the ITCZ shift in HadGEM and

Climate responses to anthropogenic emissions

L. H. Baker et al.

[Title Page](#)[Abstract](#)[Introduction](#)[Conclusions](#)[References](#)[Tables](#)[Figures](#)[Back](#)[Close](#)[Full Screen / Esc](#)[Printer-friendly Version](#)[Interactive Discussion](#)

NorESM partly explains why there are so few regions where all the models agree on the sign of precipitation change, and the model-mean responses are generally relatively weak everywhere (Fig. 7c).

There is a decrease in the multi-model mean global run-off response (Fig. 4d). All models except HadGEM show a decrease in run-off, while HadGEM shows a small increase. However, in all models there is large interannual variability in these values, so there is considerable uncertainty in these values. It is interesting to note that this decrease in run-off occurs despite a global increase in precipitation. However, the increase in precipitation occurs mostly over the ocean; regions of reduced run-off, which are mostly in the tropics and mid-latitudes, correspond to regions with reduced precipitation over land (Figs. 8b and 7c).

Overall, the climate response to removing anthropogenic BC emissions is weaker than the response to removing SO₂ emissions. Although there is a mean global temperature decrease, there is a large variation between models in the temperature response, particularly in the northern hemisphere high latitudes. All models agree on an increase in precipitation globally, although there is some variation between models in the patterns of precipitation response. There is an overall decrease in run-off, which is due to a decrease in precipitation over land, despite an increase in precipitation globally.

3.3 Response to perturbing organic carbon emissions

The multi-model mean response to removing anthropogenic OC emissions is an increase in global mean surface temperature (Fig. 4a). HadGEM and NorESM show a clear increase in surface temperature, with the largest response in HadGEM; ECHAM-HAM shows a weak reduction in global mean surface temperature, although the error bars indicate some uncertainty in the sign of this response. HadGEM and NorESM show an increase in the zonal mean surface temperature throughout the northern hemisphere, increasing towards the pole; ECHAM-HAM shows almost no change in the zonal mean surface temperature (Fig. 5f). Despite the different behaviour

Climate responses to anthropogenic emissions

L. H. Baker et al.

Title Page

Abstract

Introduction

Conclusions

References

Tables

Figures



Back

Close

Full Screen / Esc

Printer-friendly Version

Interactive Discussion



in ECHAM-HAM compared with the other models, there are broad areas where all three models agree on an increase in surface temperature, including much of the northern hemisphere mid-latitudes and some regions further north (Fig. 5e).

The TOA SW flux change is weakly positive over most of the northern hemisphere, with only a few regions where all three models agree on the sign of the change (Fig. 6e). HadGEM and NorESM show an increase in zonal mean TOA SW flux over the northern hemisphere (Fig. 6f), and in particular show increased TOA SW flux over the mid-latitudes, which have the largest anthropogenic OC emissions (Fig. 1e). In contrast, ECHAM-HAM shows a decrease in TOA SW flux over the northern hemisphere mid-latitudes (Fig. 6f). Inspection of spatial maps (not shown) indicate that this is due to decreased SW flux over Europe and the eastern USA, despite the reduced OC emissions in these regions. This may be due to natural variability in cloud cover over these regions driven by changes in atmospheric circulation patterns. The forcing signal from the OC emissions perturbation seems to be much weaker in ECHAM-HAM than in the other models, so natural variability may dominate.

The global mean precipitation changes in each model are consistent with their respective temperature responses: HadGEM and NorESM show an increase in global precipitation, while ECHAM-HAM shows a decrease (Fig. 4c). Despite the variation in temperature responses, all three models show a northward shift in the ITCZ (Fig. 7f). The changes in precipitation patterns are similar to those for the SO₂ experiments but with weaker magnitude (compare Fig. 7c and e). Run-off changes are generally small, and are driven by the change in precipitation patterns, particularly the ITCZ shift (Fig. 8c).

Overall the response to removal of anthropogenic OC emissions is an increase in surface temperature and precipitation, primarily in the northern hemisphere. The spatial patterns of changes in these quantities are broadly similar to those for the SO₂ emissions perturbation, but with smaller magnitude.

Climate responses to anthropogenic emissions

L. H. Baker et al.

[Title Page](#)[Abstract](#)[Introduction](#)[Conclusions](#)[References](#)[Tables](#)[Figures](#)[Back](#)[Close](#)[Full Screen / Esc](#)[Printer-friendly Version](#)[Interactive Discussion](#)

4 Discussion

The three models are in good agreement about the impacts of removing anthropogenic SO₂ emissions, all showing a warming concentrated in the northern hemisphere and a northward shift in the ITCZ, bringing more precipitation to the northern hemisphere.

NorESM gives a weaker overall response than the other two models. This is not surprising since NorESM is known to have a relatively low climate sensitivity (Andrews et al., 2012), which Iversen et al. (2013) attribute to a strong Atlantic Meridional Overturning Circulation in NorESM. This may explain the smaller changes in Arctic sea-ice extent changes in NorESM than in the other two models in the SO₂ experiment, reducing the impact of the additional positive feedback on temperature of the melting ice.

The response to removing anthropogenic OC emissions is similar to the that for removing SO₂, but much weaker overall. ECHAM-HAM appears to have a weaker response to the removal of OC than the other models, and this is within the range of natural variability between individual years. The other models show similar patterns of response to the SO₂ experiment, but with weaker magnitude.

In contrast, there are differences between models in their response to removing anthropogenic BC emissions: both NorESM members show a clear cooling, particularly in the Northern Hemisphere; ECHAM-HAM shows an overall cooling but some warming in the Arctic; HadGEM shows an overall warming, which is most pronounced in the northern hemisphere; and the two CAM4 members show an overall cooling but very different temperature responses in the Arctic. The stronger effects of BC removal in NorESM compared with the other models may be due to the fact that this model includes representation of the albedo effect of BC deposition on snow. This provides a mechanism to explain the stronger cooling over the Arctic in the BC experiments in this model than in the other models. When the BC emissions are reduced, less BC would be deposited on snow at high latitudes, leading to higher-albedo snow. This hypothesis is supported by the decrease in TOA SW flux over the Arctic in both NorESM members, which is consistent with an increased surface albedo, while the other models

Climate responses to anthropogenic emissions

L. H. Baker et al.

Title Page

Abstract

Introduction

Conclusions

References

Tables

Figures



Back

Close

Full Screen / Esc

Printer-friendly Version

Interactive Discussion



show mostly positive TOA SW flux change here. However, we note that the variability is large at high northern latitudes as shown by the variation between models and between the two CESM-CAM4 ensemble members. Furthermore, NorESM has a high BC abundance at mid- and high-latitudes as shown in Fig. 2. The different, and somewhat surprising, climate responses to the BC perturbations in HadGEM may be due to the fact that HadGEM has smaller amounts of BC at high altitudes in the control run than NorESM and CAM4. ECHAM-HAM also has lower amounts of high-level BC, and has a weak temperature and TOA SW flux response compared to NorESM and CAM4. The lack of high-level BC is important since the strongest direct effects of BC are from BC above clouds or other high albedo surfaces, so these effects will be much weaker in the control simulation in HadGEM and ECHAM-HAM than in the other models. Removal of anthropogenic BC emissions will therefore have a smaller impact in the models with less high-level BC since the BC forcing in the control simulation is weak to begin with. The climate responses in HadGEM may therefore be driven by natural variability (for example, the change in cloud and snow cover over Europe), which overwhelms the relatively weak forcing from the BC emissions perturbation.

The results from this study show that there is some uncertainty as to the climate response to removing anthropogenic BC emissions. The different behaviour between models is due partly to the different atmospheric BC distributions in the models. Accurately representing the correct BC distribution in GCMs is very difficult. For example, recent modifications to the convective scavenging scheme in HadGEM were designed to reduce the amount of high-level BC, which was previously too large, and this model setup gives good agreement with data from the HIPPO field campaigns in the Pacific (Wofsy, 2011); however, in other areas the results compare less well with observations, and the amount of high-level BC is probably too low in general. In contrast, NorESM and CAM4 probably have too much high-level BC compared to the HIPPO campaign observations, which overestimates the direct forcing from anthropogenic BC, and therefore exaggerates the impact of removing anthropogenic BC emissions.

Climate responses to anthropogenic emissions

L. H. Baker et al.

[Title Page](#)[Abstract](#)[Introduction](#)[Conclusions](#)[References](#)[Tables](#)[Figures](#)[Back](#)[Close](#)[Full Screen / Esc](#)[Printer-friendly Version](#)[Interactive Discussion](#)

Climate responses to anthropogenic emissions

L. H. Baker et al.

Title Page

Abstract

Introduction

Conclusions

References

Tables

Figures



Back

Close

Full Screen / Esc

Printer-friendly Version

Interactive Discussion



A further feature influencing the results in this study is the contribution of changes in sea-ice extent. Particularly for the OC and BC emissions perturbations, which give a weaker forcing than the SO₂ emissions perturbations, these sea-ice changes appear to be due to natural variability, rather than a forced response. However, they do contribute a reasonable amount to the total SW flux changes and surface temperature changes. This adds an extra element of natural variability that is not an issue in atmosphere-only simulations, which have fixed SSTs and prescribed sea-ice. This motivated our decision to perform three additional simulations, in order to increase our sample size. It can be seen from these simulations that the sea-ice responds quite differently to the BC perturbation in different simulations, even in two simulations from the same model.

It is interesting to note the range of climate responses between models, and even between different simulations run by the same model. This highlights the importance of using an ensemble of simulations in studies such as this, where natural variability is relatively large, and differences in the formulation of individual models can have a large impact on the results.

5 Conclusions

Air quality policies now and in the future will lead to reduced emissions of aerosols and other SLCPs. This study aims to evaluate the possible climate impacts of these emissions reductions, by considering a set of extreme idealised scenarios in which 100 % of the land-based anthropogenic emissions of individual aerosol precursor species (BC, OC and SO₂) are removed. The experiments were performed using three AOGCMs with interactive aerosols and chemistry, in order to capture the fast and slow responses to these emissions perturbations. We also included additional simulations from another AOGCM (without interactive aerosols) for the BC experiments.

The results show strong impacts on climate of removing SO₂ emissions, with an increase in global mean surface temperature, focussed mainly in the northern hemi-

sphere, and a northward shift in the ITCZ, driving changes in precipitation and run-off patterns, particularly in tropical regions.

The OC and BC emissions perturbations produced a much weaker signal. In both cases the models were not all in agreement on the sign of the global mean TOA SW flux change or surface temperature response. These results are different from those obtained in other studies using prescribed-SST, atmosphere-only simulations (e.g. Bellouin et al., 2015), where the forcing response to such emissions perturbations is more likely to have the same sign in all models, since the design of these experiments removes much of the variability that we see in fully-coupled AOGCMs in ocean circulation, sea-ice, atmospheric circulation changes and slow cloud responses. Overall the removal of OC emissions leads to similar patterns of response to the SO₂ experiments, but with much weaker magnitude. There is a weak northward shift in the ITCZ, and corresponding changes in run-off. The BC response is more complex, and due to the large disagreement in response between two of the models, we included three additional ensemble members. Even between two ensemble members there are large differences in the surface temperature and precipitation responses. From this study we conclude that, while BC mitigation is unlikely to be detrimental to climate, like in the case of SO₂ and OC mitigation, the climate benefits are likely to be very small, and may not be discernable above natural variability in the climate.

The Supplement related to this article is available online at doi:10.5194/acpd-15-3823-2015-supplement.

Author contributions. Model simulations were performed by L. H. Baker (HadGEM), D. J. L. Olivié (NorESM), R. Cherian (ECHAM-HAM) and Ø. Hodnebrog (CESM-CAM4). Analysis of the results was performed by L. H. Baker with contributions from D. J. L. Olivié. L. H. Baker prepared the manuscript with contributions from all co-authors.

Acknowledgements. The research leading to these results has received funding from the European Union Seventh Framework Programme (FP7/2007-2013) under grant agreement no

Climate responses to anthropogenic emissions

L. H. Baker et al.

Title Page

Abstract

Introduction

Conclusions

References

Tables

Figures



Back

Close

Full Screen / Esc

Printer-friendly Version

Interactive Discussion



282688 – ECLIPSE. The ECHAM-HAM model is developed by a consortium composed of ETH Zurich, Max Planck Institut für Meteorologie, Forschungszentrum Jülich, University of Oxford, the Finnish Meteorological Institute and the Leibniz Institute for Tropospheric Research, and managed by the Center for Climate Systems Modeling (C2SM) at ETH Zurich. R. Cherian and J. Quaas acknowledge the computing time provided by the German High Performance Computing Centre for Climate and Earth System Research (Deutsches Klimarechenzentrum, DKRZ). L. Baker and W. Collins acknowledge the use of the MONSooN supercomputing facility for running the HadGEM3 simulations.

References

- Abdul-Razzak, H. and Ghan, S. J.: A parameterization of aerosol activation: 2. Multiple aerosol types, *J. Geophys. Res.-Atmos.*, 105, 6837–6844, 2000. 3829
- Andrews, T., Forster, P. M., Boucher, O., Bellouin, N., and Jones, A.: Precipitation, radiative forcing and global temperature change, *Geophys. Res. Lett.*, 37, L14701, doi:10.1029/2010GL043991, 2010. 3827, 3836, 3839
- Andrews, T., Gregory, J. M., Webb, M. J., and Taylor, K. E.: Forcing, feedbacks and climate sensitivity in CMIP5 coupled atmosphere-ocean climate models, *Geophys. Res. Lett.*, 39, L09712, doi:10.1029/2012GL051607, 2012. 3842
- Ban-Weiss, G. A., Cao, L., Bala, G., and Caldeira, K.: Dependence of climate forcing and response on the altitude of black carbon aerosols, *Clim. Dynam.*, 38, 897–911, 2012. 3826, 3827
- Bellouin, N., Baker, L., Cherian, R., Hodnebrog, O., Olivié, D., Samset, B., MacIntosh, C., Esteve-Martinez, A., and Myhre, G.: Regional and seasonal radiative forcing by perturbations to aerosol and ozone precursor emissions, in preparation, 2015. 3828, 3845
- Bentsen, M., Bethke, I., Debernard, J. B., Iversen, T., Kirkevåg, A., Seland, Ø., Drange, H., Roelandt, C., Seierstad, I. A., Hoose, C., and Kristjánsson, J. E.: The Norwegian Earth System Model, NorESM1-M – Part 1: Description and basic evaluation of the physical climate, *Geosci. Model Dev.*, 6, 687–720, doi:10.5194/gmd-6-687-2013, 2013. 3830
- Bollasina, M. A., Ming, Y., and Ramaswamy, V.: Anthropogenic aerosols and the weakening of the South Asian summer monsoon, *Science*, 334, 502–505, 2011. 3827, 3836

Climate responses to anthropogenic emissions

L. H. Baker et al.

Title Page

Abstract

Introduction

Conclusions

References

Tables

Figures



Back

Close

Full Screen / Esc

Printer-friendly Version

Interactive Discussion



- Boucher, O., Randall, D., Artaxo, P., Bretherton, C., Feingold, G., Forster, P., Kerminen, V.-M., Kondo, Y., Liao, H., Lohmann, U., Rasch, P., Satheesh, S. K., Sherwood, S., Stevens, B., and Zhang, X.-Y.: Clouds and aerosols, in: *Climate Change 2013: The Physical Science Basis, Contribution of working group I to the fifth assessment report of the intergovernmental panel on climate change*, 571–657, Cambridge University Press, Cambridge, UK and New York, NY, USA, 2013. 3826
- 5 Ceppi, P., Hwang, Y.-T., Liu, X., Frierson, D. M., and Hartmann, D. L.: The relationship between the ITCZ and the Southern Hemispheric eddy-driven jet, *J. Geophys. Res.-Atmos.*, 118, 5136–5146, 2013. 3827
- 10 Collins, W. J., Fry, M. M., Yu, H., Fuglestedt, J. S., Shindell, D. T., and West, J. J.: Global and regional temperature-change potentials for near-term climate forcings, *Atmos. Chem. Phys.*, 13, 2471–2485, doi:10.5194/acp-13-2471-2013, 2013. 3825
- Collins, W. D.: Parameterization of generalized cloud overlap for radiative calculations in general circulation models, *J. Atmos. Sci.*, 58, 3224–3242, 2001. 3831
- 15 Danabasoglu, G., Bates, S. C., Briegleb, B. P., Jayne, S. R., Jochum, M., Large, W. G., Peacock, S., and Yeager, S. G.: The CCSM4 ocean component, *J. Climate*, 25, 1361–1389, 2012. 3831
- Edwards, J. and Slingo, A.: Studies with a flexible new radiation code. I: Choosing a configuration for a large-scale model, *Q. J. Roy. Meteor. Soc.*, 122, 689–719, 1996. 3829
- 20 Emmons, L. K., Walters, S., Hess, P. G., Lamarque, J.-F., Pfister, G. G., Fillmore, D., Granier, C., Guenther, A., Kinnison, D., Laepple, T., Orlando, J., Tie, X., Tyndall, G., Wiedinmyer, C., Baughcum, S. L., and Kloster, S.: Description and evaluation of the Model for Ozone and Related chemical Tracers, version 4 (MOZART-4), *Geosci. Model Dev.*, 3, 43–67, doi:10.5194/gmd-3-43-2010, 2010. 3831
- 25 Feichter, J., Kjellström, E., Rodhe, H., Dentener, F., Lelieveld, J., and Roelofs, G.-J.: Simulation of the tropospheric sulfur cycle in a global climate model, *Atmos. Environ.*, 30, 1693–1707, 1996. 3830
- Flanner, M. G.: Arctic climate sensitivity to local black carbon, *J. Geophys. Res.-Atmos.*, 118, 1840–1851, 2013. 3826
- 30 Flanner, M. G., Zender, C. S., Randerson, J. T., and Rasch, P. J.: Present-day climate forcing and response from black carbon in snow, *J. Geophys. Res.-Atmos.*, 112, D11202, doi:10.1029/2006JD008003, 2007. 3826

- Gedney, N., Huntingford, C., Weedon, G., Bellouin, N., Boucher, O., and Cox, P.: Detection of solar dimming and brightening effects on Northern Hemisphere river flow, *Nat. Geosci.*, 7, 796–800, 2014. 3827, 3837
- Gent, P. R., Danabasoglu, G., Donner, L. J., Holland, M. M., Hunke, E. C., Jayne, S. R., Lawrence, D. M., Neale, R. B., Rasch, P. J., Vertenstein, M., Worley, P. H., Yang, Z. L., and Zhang, M. H.: The community climate system model version 4, *J. Climate*, 24, 4973–4991, 2011. 3830, 3831
- Hewitt, H. T., Copsey, D., Culverwell, I. D., Harris, C. M., Hill, R. S. R., Keen, A. B., McLaren, A. J., and Hunke, E. C.: Design and implementation of the infrastructure of HadGEM3: the next-generation Met Office climate modelling system, *Geosci. Model Dev.*, 4, 223–253, doi:10.5194/gmd-4-223-2011, 2011. 3829
- HTAP: Hemispheric Transport of Air Pollution 2010 – Part A: Ozone and Particulate Matter, Air Pollution Studies No. 17, edited by: Dentener, F., Keating, T., and Akimoto, H., United Nations, New York and Geneva, 2010. 3825
- Hunke, E. C. and Lipscomb, W. H.: CICE: the Los Alamos Sea Ice Model Documentation and Software User’s Manual Version 4.0 LA-CC-06-012, 2008. 3829, 3831
- Iversen, T., Bentsen, M., Bethke, I., Debernard, J. B., Kirkevåg, A., Seland, Ø., Drange, H., Kristjansson, J. E., Medhaug, I., Sand, M., and Seierstad, I. A.: The Norwegian Earth System Model, NorESM1-M – Part 2: Climate response and scenario projections, *Geosci. Model Dev.*, 6, 389–415, doi:10.5194/gmd-6-389-2013, 2013. 3830, 3842
- Jungclaus, J., Fischer, N., Haak, H., Lohmann, K., Marotzke, J., Matei, D., Mikolajewicz, U., Notz, D., and Storch, J.: Characteristics of the ocean simulations in the Max Planck Institute Ocean Model (MPIOM) the ocean component of the MPI-Earth system model, *Journal of Advances in Modeling Earth Systems*, 5, 422–446, 2013. 3830
- Kang, S. M., Held, I. M., Frierson, D. M., and Zhao, M.: The response of the ITCZ to extratropical thermal forcing: idealized slab-ocean experiments with a GCM, *J. Climate*, 21, 3521–3532, 2008. 3827
- Kirkevåg, A., Iversen, T., Seland, Ø., Hoose, C., Kristjansson, J. E., Struthers, H., Ekman, A. M. L., Ghan, S., Griesfeller, J., Nilsson, E. D., and Schulz, M.: Aerosol–climate interactions in the Norwegian Earth System Model – NorESM1-M, *Geosci. Model Dev.*, 6, 207–244, doi:10.5194/gmd-6-207-2013, 2013. 3830
- Klimont, Z., Smith, S. J., and Cofala, J.: The last decade of global anthropogenic sulfur dioxide: 2000–2011 emissions, *Environ. Res. Lett.*, 8, 014003, 2013. 3832

Climate responses to anthropogenic emissions

L. H. Baker et al.

[Title Page](#)[Abstract](#)[Introduction](#)[Conclusions](#)[References](#)[Tables](#)[Figures](#)[Back](#)[Close](#)[Full Screen / Esc](#)[Printer-friendly Version](#)[Interactive Discussion](#)

Climate responses to anthropogenic emissions

L. H. Baker et al.

Title Page

Abstract

Introduction

Conclusions

References

Tables

Figures



Back

Close

Full Screen / Esc

Printer-friendly Version

Interactive Discussion



- Klimont, Z., Kupiainen, K., Heyes, C., Purohit, P., Cofala, J., Rafaj, P., and Schoepp, W.: Global anthropogenic emissions of particulate matter, in preparation, 2015. 3832
- Koch, D. and Del Genio, A. D.: Black carbon semi-direct effects on cloud cover: review and synthesis, *Atmos. Chem. Phys.*, 10, 7685–7696, doi:10.5194/acp-10-7685-2010, 2010. 3826
- 5 Kristjánsson, J., Iversen, T., Kirkevåg, A., Seland, Ø., and Debernard, J.: Response of the climate system to aerosol direct and indirect forcing: role of cloud feedbacks, *J. Geophys. Res.-Atmos.*, 110, D24206, doi:10.1029/2005JD006299, 2005. 3826, 3832
- Kvalevåg, M. M., Samset, B. H., and Myhre, G.: Hydrological sensitivity to greenhouse gases and aerosols in a global climate model, *Geophys. Res. Lett.*, 40, 1432–1438, 2013. 3827
- 10 Lambert, F. H. and Webb, M. J.: Dependency of global mean precipitation on surface temperature, *Geophys. Res. Lett.*, 35, L16706, doi:10.1029/2008GL034838, 2008. 3826
- Lawrence, D. M., Oleson, K. W., Flanner, M. G., Thornton, P. E., Swenson, S. C., Lawrence, P. J., Zeng, X., Yang, Z.-L., Levis, S., Sakaguchi, K., Bonan, G. B., and Slater, A. G.: Parameterization improvements and functional and structural advances in version 4 of the Community Land Model, *Journal of Advances in Modeling Earth Systems*, 3, M03001, doi:10.1029/2011MS00045, 2011. 3831
- 15 Lohmann, U., Stier, P., Hoose, C., Ferrachat, S., Kloster, S., Roeckner, E., and Zhang, J.: Cloud microphysics and aerosol indirect effects in the global climate model ECHAM5-HAM, *Atmos. Chem. Phys.*, 7, 3425–3446, doi:10.5194/acp-7-3425-2007, 2007. 3830
- 20 Mann, G. W., Carslaw, K. S., Spracklen, D. V., Ridley, D. A., Manktelow, P. T., Chipperfield, M. P., Pickering, S. J., and Johnson, C. E.: Description and evaluation of GLOMAP-mode: a modal global aerosol microphysics model for the UKCA composition-climate model, *Geosci. Model Dev.*, 3, 519–551, doi:10.5194/gmd-3-519-2010, 2010. 3829
- Ming, Y. and Ramaswamy, V.: Nonlinear climate and hydrological responses to aerosol effects, *J. Climate*, 22, 1329–1339, 2009. 3827
- 25 Ming, Y., Ramaswamy, V., and Persad, G.: Two opposing effects of absorbing aerosols on global-mean precipitation, *Geophys. Res. Lett.*, 37, L13701, doi:10.1029/2010GL042895, 2010. 3826, 3827
- 30 Myhre, G., Berglen, T. F., Johnsrud, M., Hoyle, C. R., Berntsen, T. K., Christopher, S. A., Fahey, D. W., Isaksen, I. S. A., Jones, T. A., Kahn, R. A., Loeb, N., Quinn, P., Remer, L., Schwarz, J. P., and Yttri, K. E.: Modelled radiative forcing of the direct aerosol effect with multi-observation evaluation, *Atmos. Chem. Phys.*, 9, 1365–1392, doi:10.5194/acp-9-1365-2009, 2009. 3831

Climate responses to anthropogenic emissions

L. H. Baker et al.

Title Page

Abstract

Introduction

Conclusions

References

Tables

Figures



Back

Close

Full Screen / Esc

Printer-friendly Version

Interactive Discussion



Neale, R., Richter, J., Conley, A., Park, S., Lauritzen, P., Gettelm, A., Williamson, D., Rasch, P., Vavrus, S., Taylor, M., Collins, W., Zhang, M., and Lin, S.-J.: Description of the NCAR Community Atmosphere Model (CAM 4.0), Tech. rep., National Center for Atmospheric Research (NCAR), Boulder, Colorado, 2011. 3830, 3831

5 Neale, R. B., Richter, J., Park, S., Lauritzen, P. H., Vavrus, S. J., Rasch, P. J., and Zhang, M.: The mean climate of the Community Atmosphere Model (CAM4) in forced SST and fully coupled experiments, *J. Climate*, 26, 5150–5168, 2013. 3830

O'Connor, F. M., Johnson, C. E., Morgenstern, O., Abraham, N. L., Braesicke, P., Dalvi, M., Folberth, G. A., Sanderson, M. G., Telford, P. J., Voulgarakis, A., Young, P. J., Zeng, G.,
10 Collins, W. J., and Pyle, J. A.: Evaluation of the new UKCA climate-composition model – Part 2: The Troposphere, *Geosci. Model Dev.*, 7, 41–91, doi:10.5194/gmd-7-41-2014, 2014. 3829

Olivié, D., Peters, G., and Saint-Martin, D.: Atmosphere response time scales estimated from AOGCM experiments, *J. Climate*, 25, 7956–7972, 2012. 3832

Pausata, F. S. R., Gaetani, M., Messori, G., Kloster, S., and Dentener, F. J.: The role of aerosol
15 in altering North Atlantic atmospheric circulation in winter and air-quality feedbacks, *Atmos. Chem. Phys. Discuss.*, 14, 22477–22506, doi:10.5194/acpd-14-22477-2014, 2014. 3832

Polson, D., Bollasina, M., Hegerl, G., and Wilcox, L.: Decreased monsoon precipitation in the Northern Hemisphere due to anthropogenic aerosols, *Geophys. Res. Lett.*, 41, 6023–6029,
20 doi:10.1002/2014GL060811, 2014. 3827, 3836

Ramanathan, V. and Carmichael, G.: Global and regional climate changes due to black carbon, *Nat. Geosci.*, 1, 221–227, 2008. 3826

Rosenfeld, D., Lohmann, U., Raga, G. B., O'Dowd, C. D., Kulmala, M., Fuzzi, S., Reissell, A., and Andreae, M. O.: Flood or drought: how do aerosols affect precipitation?, *Science*, 321,
25 1309–1313, 2008. 3827

Sand, M., Berntsen, T. K., Kay, J. E., Lamarque, J. F., Seland, Ø., and Kirkevåg, A.: The Arctic response to remote and local forcing of black carbon, *Atmos. Chem. Phys.*, 13, 211–224,
doi:10.5194/acp-13-211-2013, 2013a. 3826

Sand, M., Berntsen, T. K., Seland, Ø., and Kristjánsson, J. E.: Arctic surface temperature change to emissions of black carbon within Arctic or midlatitudes, *J. Geophys. Res.-Atmos.*,
30 118, 7788–7798, 2013b. 3826

Shindell, D. and Faluvegi, G.: Climate response to regional radiative forcing during the twentieth century, *Nat. Geosci.*, 2, 294–300, 2009. 3825

Climate responses to anthropogenic emissions

L. H. Baker et al.

Title Page

Abstract

Introduction

Conclusions

References

Tables

Figures



Back

Close

Full Screen / Esc

Printer-friendly Version

Interactive Discussion



- Shindell, D. T.: Inhomogeneous forcing and transient climate sensitivity, *Nature Climate Change*, 4, 274–277, doi:10.1038/nclimate2136, 2014. 3825
- Shindell, D. T., Faluvegi, G., Koch, D. M., Schmidt, G. A., Unger, N., and Bauer, S. E.: Improved attribution of climate forcing to emissions, *Science*, 326, 716–718, 2009. 3825
- 5 Smith, R., Jones, P., Briegleb, B., Bryan, F., Danabasoglu, G., Dennis, J., Dukowicz, J., Eden, C., Fox-Kemper, B., Gent, P., Hecht, M., Jayne, S., Jochum, M., Large, W., Lindsay, K., Maltrud, M., Norton, N., Peacock, S., Vertenstein, M., and Yeager, S.: The Parallel Ocean Program (POP) reference manual: Ocean component of the Community Climate System Model (CCSM), Los Alamos National Laboratory, LAUR-10-01853, 2010. 3831
- 10 Søvde, O. A., Gauss, M., Smyshlyaev, S. P., and Isaksen, I. S.: Evaluation of the chemical transport model Oslo CTM2 with focus on arctic winter ozone depletion, *J. Geophys. Res.-Atmos.*, 113, D09304, doi:10.1029/2007JD009240, 2008. 3831
- Stevens, B., Giorgetta, M., Esch, M., Mauritsen, T., Crueger, T., Rast, S., Salzmann, M., Schmidt, H., Bader, J., Block, K., Brokopf, R., Fast, I., Kinne, S., Kornblueh, L., Lohmann, U., Pincus, R., Reichler, T., and Roeckner, E.: Atmospheric component of the MPI-M Earth System Model: ECHAM6, *Journal of Advances in Modeling Earth Systems*, 5, 146–172, 2013. 3829
- 15 Stier, P., Feichter, J., Kinne, S., Kloster, S., Vignati, E., Wilson, J., Ganzeveld, L., Tegen, I., Werner, M., Balkanski, Y., Schulz, M., Boucher, O., Minikin, A., and Petzold, A.: The aerosol-climate model ECHAM5-HAM, *Atmos. Chem. Phys.*, 5, 1125–1156, doi:10.5194/acp-5-1125-2005, 2005. 3830
- 20 Textor, C., Schulz, M., Guibert, S., Kinne, S., Balkanski, Y., Bauer, S., Berntsen, T., Berglen, T., Boucher, O., Chin, M., Dentener, F., Diehl, T., Feichter, J., Fillmore, D., Ginoux, P., Gong, S., Grini, A., Hendricks, J., Horowitz, L., Huang, P., Isaksen, I. S. A., Iversen, T., Kloster, S., Koch, D., Kirkevåg, A., Kristjansson, J. E., Krol, M., Lauer, A., Lamarque, J. F., Liu, X., Montanaro, V., Myhre, G., Penner, J. E., Pitari, G., Reddy, M. S., Seland, Ø., Stier, P., Takemura, T., and Tie, X.: The effect of harmonized emissions on aerosol properties in global models – an AeroCom experiment, *Atmos. Chem. Phys.*, 7, 4489–4501, doi:10.5194/acp-7-4489-2007, 2007. 3833
- 25 Vignati, E., Wilson, J., and Stier, P.: M7: an efficient size-resolved aerosol microphysics module for large-scale aerosol transport models, *J. Geophys. Res.-Atmos.*, 109, D22202, doi:10.1029/2003JD004485, 2004. 3830
- 30

- Wang, Y., Wang, M., Zhang, R., Ghan, S. J., Lin, Y., Hu, J., Pan, B., Levy, M., Jiang, J. H., and Molina, M. J.: Assessing the effects of anthropogenic aerosols on Pacific storm track using a multiscale global climate model, *P. Natl. Acad. Sci. USA*, 111, 6894–6899, 2014. 3835
- 5 Wofsy, S.: HIAPER Pole-to-Pole Observations (HIPPO): fine-grained, global-scale measurements of climatically important atmospheric gases and aerosols, *Philos. T. R. Soc. A*, 369, 2073–2086, 2011. 3843
- 10 Zhang, K., O'Donnell, D., Kazil, J., Stier, P., Kinne, S., Lohmann, U., Ferrachat, S., Croft, B., Quaas, J., Wan, H., Rast, S., and Feichter, J.: The global aerosol-climate model ECHAM-HAM, version 2: sensitivity to improvements in process representations, *Atmos. Chem. Phys.*, 12, 8911–8949, doi:10.5194/acp-12-8911-2012, 2012. 3830

Climate responses to anthropogenic emissions

L. H. Baker et al.

[Title Page](#)[Abstract](#)[Introduction](#)[Conclusions](#)[References](#)[Tables](#)[Figures](#)[Back](#)[Close](#)[Full Screen / Esc](#)[Printer-friendly Version](#)[Interactive Discussion](#)

Climate responses to anthropogenic emissions

L. H. Baker et al.

Title Page

Abstract

Introduction

Conclusions

References

Tables

Figures



Back

Close

Full Screen / Esc

Printer-friendly Version

Interactive Discussion



Table 1. Summary of BC and OC burdens in the control simulation for the three models.

	HadGEM	ECHAM-HAM	NorESM	CAM4
BC burden (Tg)	0.080	0.102	0.163	0.144
OC burden (Tg)	0.734	0.769	1.047	0.601
SO ₄ burden (Tg)	3.355	5.345	1.813	1.918

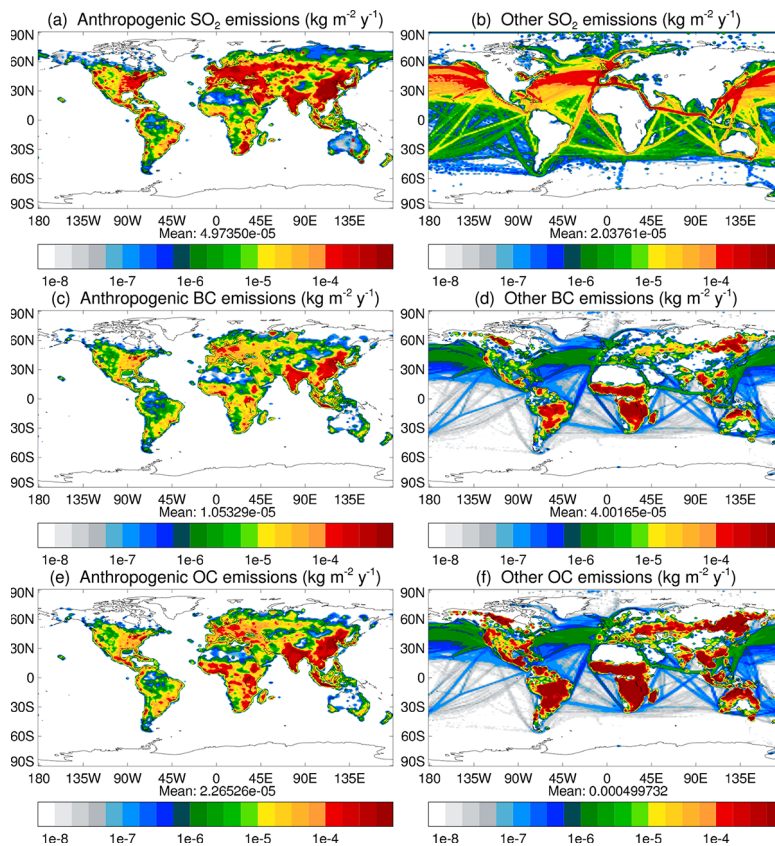


Figure 1. Emissions of aerosol and aerosol precursor species. **(a, b):** SO₂; **(c, d):** BC; and **(e, f):** OC emissions. Left column: anthropogenic emissions, which are perturbed in the respective experiments. Right column: natural, biomass burning (for the year 2008) and shipping emissions, which are not perturbed in these experiments.

Climate responses to anthropogenic emissions

L. H. Baker et al.

Title Page

Abstract Introduction

Conclusions References

Tables Figures

◀ ▶

◀ ▶

Back Close

Full Screen / Esc

Printer-friendly Version

Interactive Discussion



Climate responses to anthropogenic emissions

L. H. Baker et al.

Title Page

Abstract

Introduction

Conclusions

References

Tables

Figures



Back

Close

Full Screen / Esc

Printer-friendly Version

Interactive Discussion

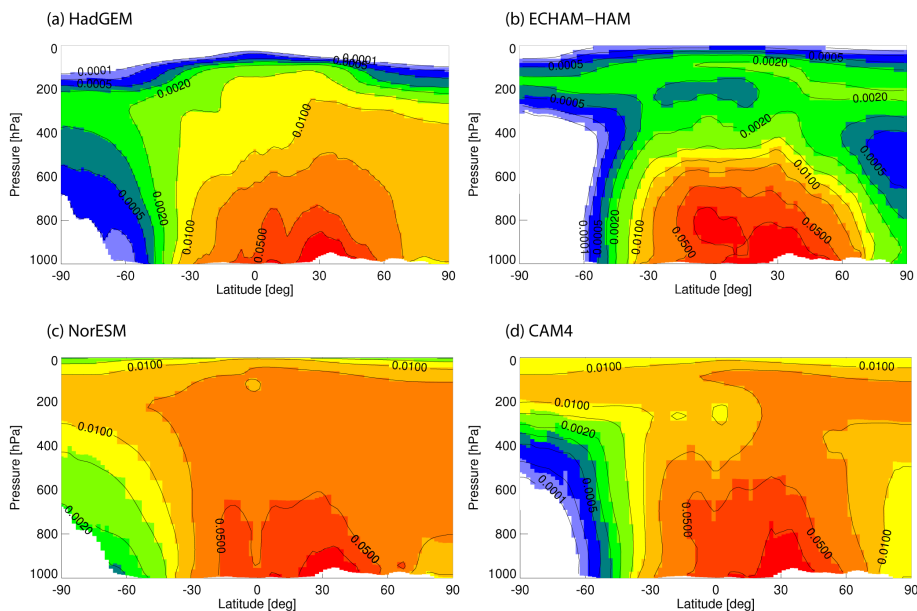


Figure 2. Annual average zonal mean BC mass mixing ratio ($\mu\text{g kg}^{-1}$) in the control simulation for each model. **(a)** HadGEM, **(b)** ECHAM-HAM, **(c)** NorESM and **(d)** CAM4.

Climate responses to anthropogenic emissions

L. H. Baker et al.

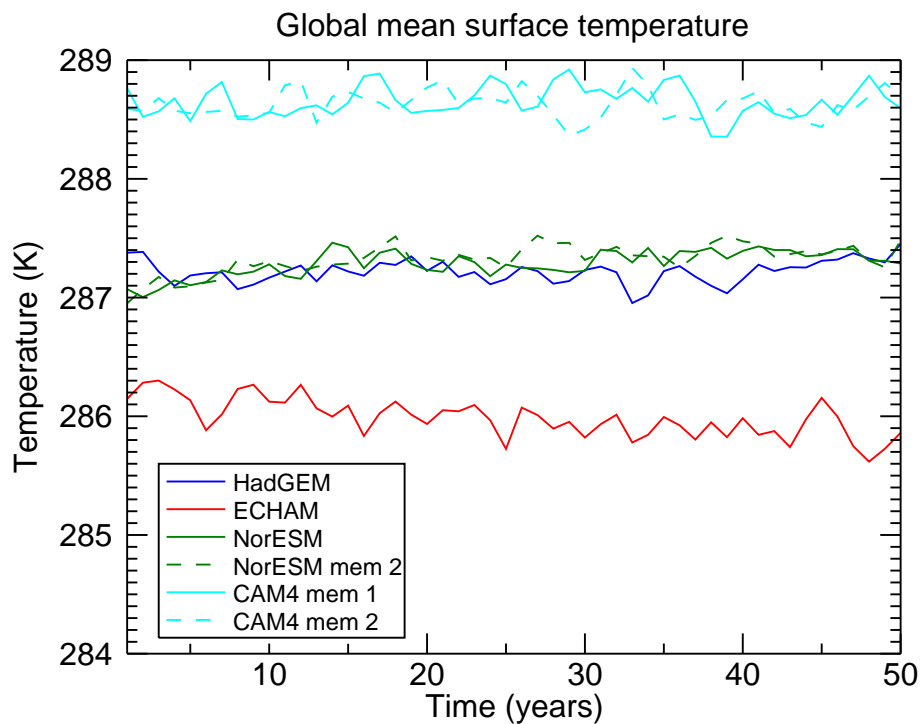


Figure 3. Time evolution of global mean annual average temperature in the control simulation for each model.

[Title Page](#)[Abstract](#)[Introduction](#)[Conclusions](#)[References](#)[Tables](#)[Figures](#)[Back](#)[Close](#)[Full Screen / Esc](#)[Printer-friendly Version](#)[Interactive Discussion](#)

Climate responses to anthropogenic emissions

L. H. Baker et al.

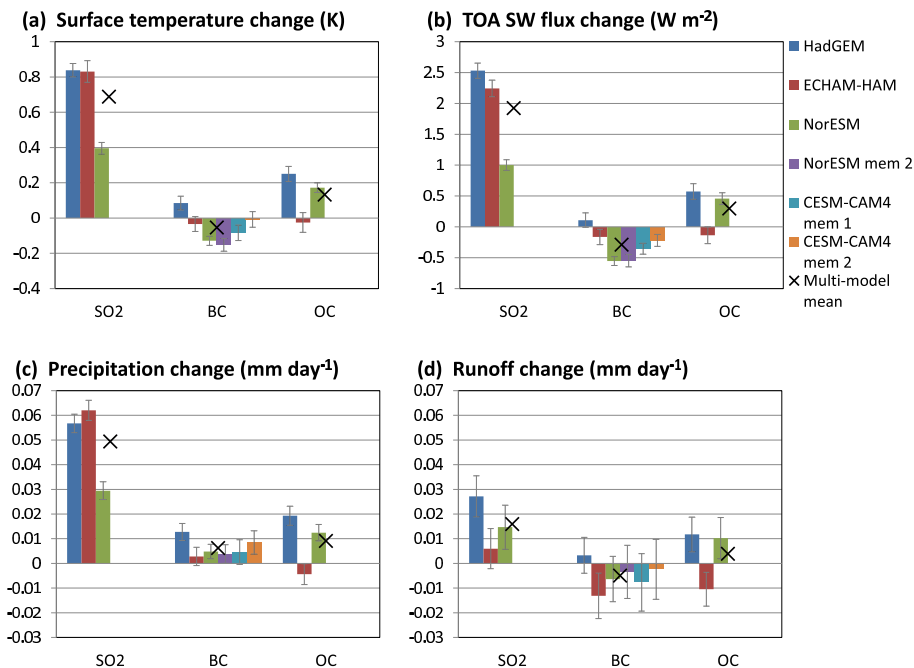


Figure 4. Summary of global mean annual average changes in **(a)** surface temperature, **(b)** TOA SW flux, **(c)** precipitation and **(d)** run-off. The error bars indicate the 95 % confidence interval on the error in the mean ($2\sigma/\sqrt{n}$, where n is 50 yr).

Title Page

Abstract Introduction

Conclusions References

Tables Figures

◀ ▶

◀ ▶

Back Close

Full Screen / Esc

Printer-friendly Version

Interactive Discussion



Climate responses to anthropogenic emissions

L. H. Baker et al.

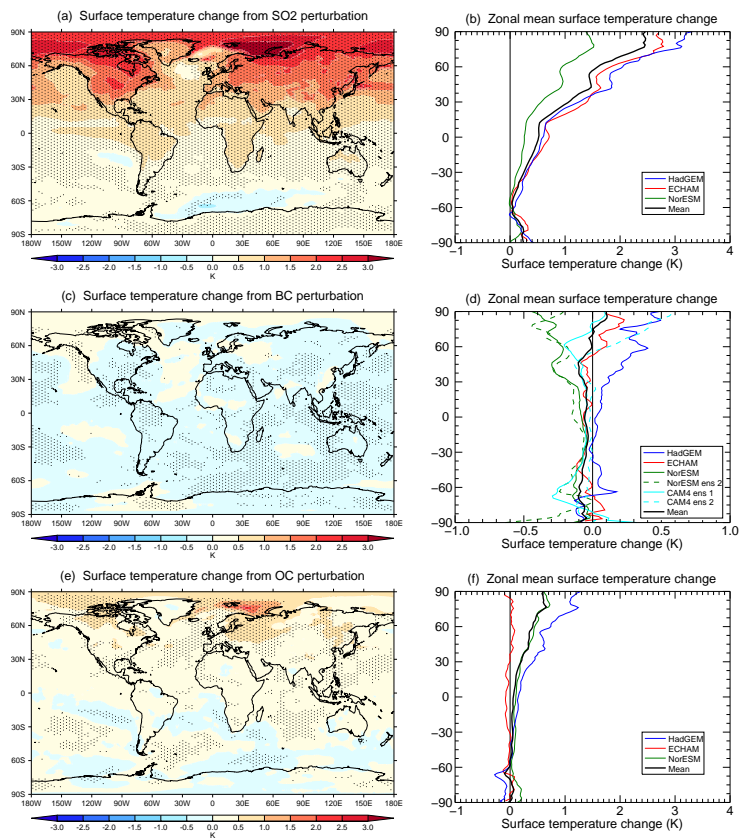


Figure 5. Annual average change in surface temperature for **(a, b)** SO_2 , **(c, d)** BC and **(e, f)** OC perturbations. Left column: multi-model mean maps. Right column: zonal mean. In **(a, e)**, stippling shows points where all three models agree on the sign of the response. In **(c)** stippling shows points where at least five of the six model simulations agree on the sign.

Climate responses to anthropogenic emissions

L. H. Baker et al.

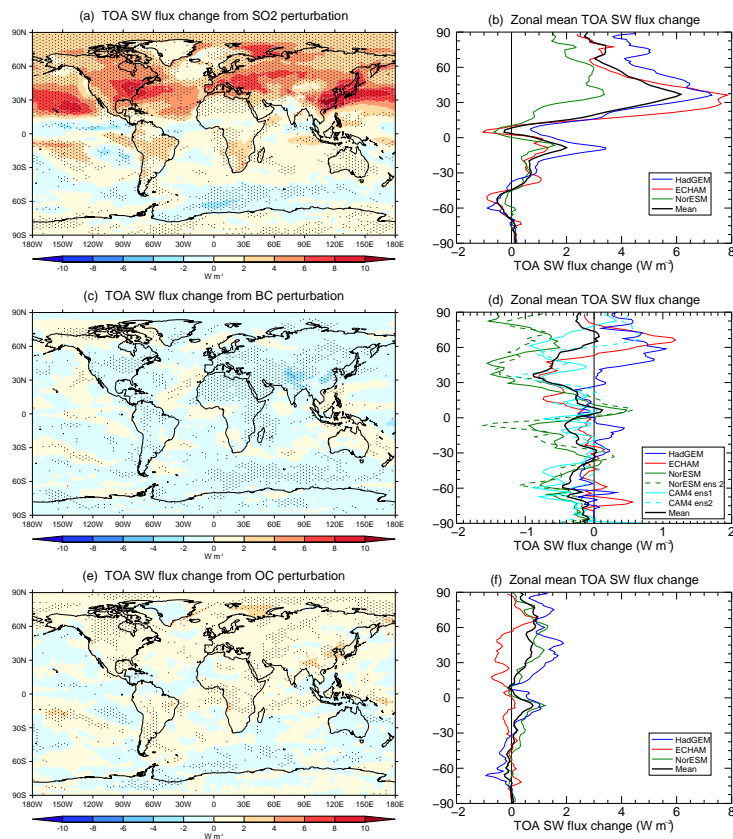


Figure 6. Annual average change in TOA SW flux for (a, b) SO_2 , (c, d) BC and (e, f) OC perturbations. Left column: multi-model mean maps. Right column: zonal mean. In (a, e), stippling shows points where all three models agree on the sign of the response. In (c) stippling shows points where at least five of the six model simulations agree on the sign.

Climate responses to anthropogenic emissions

L. H. Baker et al.

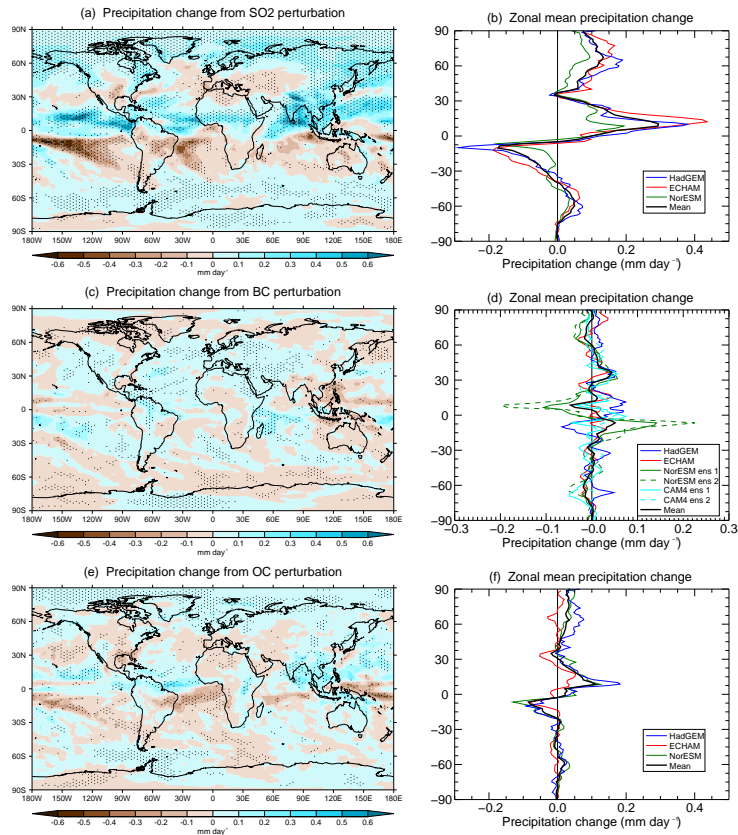


Figure 7. Annual average change in precipitation for (a, b) SO₂, (c, d) BC and (e, f) OC perturbations. Left column: multi-model mean maps. Right column: zonal mean. In (a, e), stippling shows points where all three models agree on the sign of the response. In (c) stippling shows points where at least five of the six model simulations agree on the sign.

Title Page

Abstract

Introduction

Conclusions

References

Tables

Figures



Back

Close

Full Screen / Esc

Printer-friendly Version

Interactive Discussion



Climate responses to anthropogenic emissions

L. H. Baker et al.

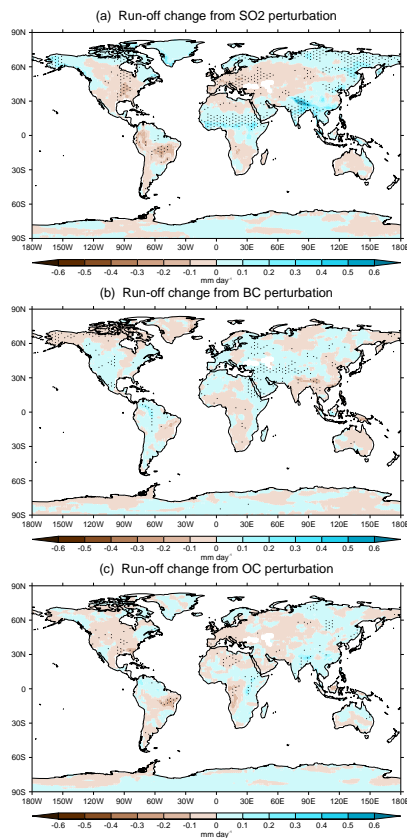


Figure 8. Multi-model mean maps of annual average change in run-off for **(a)** SO₂, **(b)** BC and **(c)** OC perturbations. In **(a, c)**, stippling shows points where all three models agree on the sign of the response. In **(b)** stippling shows points where at least five of the six model simulations agree on the sign.

[Title Page](#)[Abstract](#)[Introduction](#)[Conclusions](#)[References](#)[Tables](#)[Figures](#)[Back](#)[Close](#)[Full Screen / Esc](#)[Printer-friendly Version](#)[Interactive Discussion](#)